Data and analytical mechanics: a new look on NATM tunnels

Raphael Scharf, Bernhard Pichler, Christian Hellmich
Institute for Mechanics of Materials and Structures, TU Wien (Vienna University of Technology), Vienna, Austria

Roman Heissenberger, Bernd Moritz
ÖBB - Infrastruktur AG, Streckenmanagement und Anlagenentwicklung, Fachbereich Bautechnik - Tunnelbau, Graz, Austria

ABSTRACT: Hybrid methods, i.e. combinations of deformation measurements with structural and material mechanics have been successfully used, for more than 20 years, for the New Austrian Tunneling Method (NATM), and beyond. This contribution extends these developments with respect to the mechanical behavior of such structures for more efficient evaluation of long-term behavior. In detail, internal shell-specific forces derived from the principle of virtual power are analytically linked, based on an aging viscoelastic material model, to radial and circumferential displacement components which were measured at selected points of the tunnel shell. For the Sieberg tunnel the data-driven analytical mechanics model evidences virtually uniform ground pressure distributions, leading to a first rapidly increasing, and then mildly decreasing utilization degree of the shotcrete shell.

Keywords: analytical mechanics, New Austrian Tunneling Method, aging viscoelasticity, shotcrete.

1 INTRODUCTION

In tunnel engineering, unlike traditional structural engineering, the external loads that the tunnel has to resist are not known *a priori*. Instead, displacements of selected points of the inner surface of the tunnel lining are known, because they are standardly measured (Moritz et al. 2023), as part of structural monitoring during the construction phase, nowadays typically by means of methods from laser optical geodesy. Therefore, as a rule, both the loads acting on the tunnel lining and the stress states in the tunnel lining need to be estimated from the aforementioned displacement measurements.

The present contribution deals with (non-closed) top headings made of hydrating shotcrete in the framework of the New Austrian Tunneling Method (NATM), monitored by geodetic displacement measurements at three points. We explicitly introduce the outer surface of the tunnel shell, on which normal traction forces ("ground pressure") will be imposed, while the equilibrium of forces within each cross-sectional plane of the tunnel shell will be maintained by normal tractions ("impost forces") acting on the footings of the tunnel shell segments.

2 ANALYTICAL MECHANICS OF AGING VISCOELASTIC SHOTCRETE TUNNEL SHELLS

Aiming at both efficiency and transparency of computational procedures for tunnel safety assessment, we here develop semi-analytical formulae resting on the principle of virtual power (Germain 1972, 1973), aging viscoelasticity (Scheiner and Hellmich, 2009), and suitably chosen load distribution functions for an NATM tunnel shell.

2.1 Cross-sectional equilibrium within an arch-like tunnel cross-section: application of the principle of virtual power

For the cross-sectional equilibrium within an arch-like tunnel cross-section, the so-called principle of virtual power (Germain 1972, 1973), was used in (Scharf et al. 2022), which leads to the following differential equilibrium conditions valid along the entire arch segment

$$-n_\varphi + \frac{1}{R}\frac{\mathrm{d}^2 m_\varphi}{\mathrm{d}\varphi^2} - R\,G_p = 0, \quad \text{and} \quad \frac{\mathrm{d}n_\varphi}{\mathrm{d}\varphi} + \frac{1}{R}\frac{\mathrm{d}m_\varphi}{\mathrm{d}\varphi} = 0 \quad \text{for} \quad \varphi_b \le \varphi \le \varphi_e \tag{1}$$

with the axial forces n_φ, the bending moment m_φ, and the ground pressure G_p. In addition, the principle of virtual power gives access to the natural boundary condition which guarantee equilibrium at the beginning and at the end of the tunnel segment,

$$\text{for} \quad \varphi = \varphi_b \quad \text{and} \quad \varphi = \varphi_e\text{:} \quad -\frac{1}{R}\frac{\mathrm{d}m_\varphi}{\mathrm{d}\varphi} = 0 \tag{2}$$

so that the forces of the tunnel shell are in equilibrium. These differential equations can be solved for given functions quantifying the ground pressure distribution. This leads to ground pressure-induced distributions of internal axial forces and bending moments in tunnel shell segment, see (Scharf et al. 2022), using the following boundary conditions

$$N_{p,b} = -n_\varphi(\varphi_b), \quad N_{p,e} = -n_\varphi(\varphi_e), \quad m_\varphi(\varphi_b) = 0, \quad m_\varphi(\varphi_e) = 0, \tag{3}$$

where, independent of the ground pressure distribution, for the fulfillment of $(3)_4$ the impost forces at the beginning and the end of tunnel segment $N_{p,b}$, $N_{p,e}$ have to be equal, i.e. $N_{p,b} = N_{p,e} = N_p$.

2.2 Aging and nonlinear creep of shotcrete shells

For the (ultra-)short term creep of shotcrete, the following power law is used by analogy to (Irfan-ul Hasan et al. 2016), (Königsberger et al. 2016)

$$J(\xi, t) = \frac{1}{E(\xi)} + \frac{1}{E_c(\xi)}\left[\frac{t}{t_0^*}\right]^\beta \tag{4}$$

with the power-law exponent amounting typically to 0.25 (Königsberger et al. 2016), and with $t_0^* = 1$ d as a reference time. The temporal evolution of the elastic modulus E and creep modulus E_c as well for the uniaxial compressive strength of shotcrete f_c under isothermal conditions at 20°C are approximate by suitable fitting functions, such as given in (Ausweger et al. 2019). However, the degree of hydration also evolves with time, so strictly speaking, (4) is only valid for a very short time interval in which the degree of hydration ξ is virtually constant. Therefore, according to (Scheiner & Hellmich 2009), the constitutive relations need to be transformed into a rate form.

Moreover, it is known that the creep compliance increases non-linearly with the stress once a critical load level is exceeded. This is elegantly quantified in terms of the affinity concept of (Ruiz et al. 2007), according to which the rate of the creep function needs to be multiplied by factor η

$$\frac{\partial J^{\mathrm{NL}}}{\partial t} = \eta\,\frac{\partial J}{\partial t} \quad \text{with} \quad \eta = 1 + 2\mathcal{L}^4 \quad \text{for} \quad \mathcal{L} > 0 \tag{5}$$

The level of loading $\mathcal{L}$ relative to the strength of the material is described with a Drucker-Prager strength criterion, applied to the stresses at the center line of the tunnel shell, see (Scharf et al. 2022).

2.3 Displacement and rotation rates across the tunnel segment

When choosing suitable functions for the spatial distribution of the normal traction forces ("ground pressure") acting on the tunnel shell, namely the polynomials reported in (Scharf et al. 2022), combination of equilibrium conditions (Eqs. (1)-(3)) and material behavior (Eq. (4)) allows for derivation of displacement and rotation rates across the tunnel shell, as functions of the outer forces acting on it. As given in detail in (Scharf et al. 2022), this deformation-force relations read as

$$\begin{aligned}+\dot{u}_r^C(\xi,\overline{\varphi},t) - R\dot{\theta}_{z,b}^C(t)\sin(\overline{\varphi}) - \dot{u}_{\varphi,b}^C(t)\sin(\overline{\varphi}) - \dot{u}_{r,b}^C(t)\cos(\overline{\varphi}) \\ = +\mathcal{I}_{N\to r}(\overline{\varphi})\left[\frac{\dot{N}_p(t)}{E(\xi(t))} + \int_0^t \frac{\partial J}{\partial t}(\xi(t), t-\tau)\dot{N}_p(\tau)\,\mathrm{d}\tau\right] \\ + \sum_{i=1}^{4}\left\{\mathcal{I}_{i\to r}(\overline{\varphi})\left[\frac{\dot{G}_{p,i}(t)}{E(\xi(t))} + \int_0^t \frac{\partial J}{\partial t}(\xi(t), t-\tau)\dot{G}_{p,i}(\tau)\,\mathrm{d}\tau\right]\right\}\end{aligned} \tag{6}$$

$$\begin{aligned}+\dot{u}_\varphi^C(\xi,\overline{\varphi},t) - R\dot{\theta}_{z,b}^C(t)\{\cos(\overline{\varphi})-1\} - \dot{u}_{\varphi,b}^C(t)\cos(\overline{\varphi}) + \dot{u}_{r,b}^C(t)\sin(\overline{\varphi}) \\ = +\mathcal{I}_{N\to\varphi}(\overline{\varphi})\left[\frac{\dot{N}_p(t)}{E(\xi(t))} + \int_0^t \frac{\partial J}{\partial t}(\xi(t), t-\tau)\dot{N}_p(\tau)\mathrm{d}\tau\right] \\ + \sum_{i=1}^{4}\left\{\mathcal{I}_{i\to\varphi}(\overline{\varphi})\left[\frac{\dot{G}_{p,i}(t)}{E(\xi(t))} + \int_0^t \frac{\partial J}{\partial t}(\xi(t), t-\tau)\dot{G}_{p,i}(\tau)\mathrm{d}\tau\right]\right\}\end{aligned} \tag{7}$$

$$\begin{aligned}+\dot{\theta}_z^C(\xi,\overline{\varphi},t) - \dot{\theta}_{z,b}^C(t) \\ = +\mathcal{I}_{N\to z}(\overline{\varphi})\left[\frac{\dot{N}_p(t)}{E(\xi(t))} + \int_0^t \frac{\partial J}{\partial t}(\xi(t), t-\tau)\dot{N}_p(\tau)\mathrm{d}\tau\right] \\ + \sum_{i=1}^{4}\left\{\mathcal{I}_{i\to z}(\overline{\varphi})\left[\frac{\dot{G}_{p,i}(t)}{E(\xi(t))} + \int_0^t \frac{\partial J}{\partial t}(\xi(t), t-\tau)\dot{G}_{p,i}(\tau)\mathrm{d}\tau\right]\right\}\end{aligned} \tag{8}$$

with the radial and circumferential displacement rates $\dot{u}_r^C$, $\dot{u}_\varphi^C$, the rate of the rotational angle $\dot{\theta}_z^C$, and their values at the beginning of the shell $\dot{u}_{r,b}^C$, $\dot{u}_{\varphi,b}^C$, and $\dot{\theta}_{z,b}^C$; the rate of the impost forces $\dot{N}_p$ and the ground pressures $\dot{G}_{p,i}$; and with the time-invariant influence functions $\mathcal{I}$ given as Eqs.(99)-(113) in (Scharf et al. 2022), the elastic modulus E, the creep function J, and the degree of hydration ξ.

3 TEMPORAL LINEAR DISCRETIZATION OF THE DISPLACEMENT-TO-FORCE CONVERSION

The conversion of displacements measured in the measurement points into compressive traction forces acting on the outer shell surface and on the imposts is based on a temporally discretized version of Eqs. (6)-(8). Between chosen time instants since the installation of the top heading, the temporal evolutions of the displacements and rotational angles are approximated linearly, so that the corresponding rates become constants during the time intervals $[t_n, t_{n+1}]$. The same type of temporal approximation is used for the ground and impost pressure values. Mathematically, this reads as

$$\dot{x}(\Delta t_{n+1}) = \frac{x(t_{n+1}) - x(t_n)}{\Delta t_{n+1}} \quad \text{with} \quad \Delta t_{n+1} = t_{n+1} - t_n \tag{9}$$

Finally, also the same type of temporal approximation is used for the material properties, so that

$$E(t) = E\big(\xi(t_n)\big) + \frac{t-t_n}{\Delta t_{n+1}}\big[E\big(\xi(t_{n+1})\big) - E\big(\xi(t_n)\big)\big] \tag{10}$$

$$\begin{aligned}\frac{\partial J^{\mathrm{NL}}}{\partial t}(t) = \frac{\partial J^{\mathrm{NL}}}{\partial t}(\xi(t_n), t-t_n) \\ + \frac{t-t_n}{\Delta t_{n+1}}\left[\frac{\partial J^{\mathrm{NL}}}{\partial t}(\xi(t_{n+1}), t-t_n) - \frac{\partial J^{\mathrm{NL}}}{\partial t}(\xi(t_n), t-t_n)\right]\end{aligned} \tag{11}$$

Using (9)-(11) in the rate equations (6)-(8) gives the following discrete format for the increments of radial and tangential displacements and of rotational angles, respectively,

$$
\begin{aligned}
&+\frac{u_r^C(\xi,\overline{\varphi},t_{n+1})-u_r^C(\xi,\overline{\varphi},t_n)}{\Delta t_{n+1}}-\frac{u_{r,b}^C(t_{n+1})-u_{r,b}^C(t_n)}{\Delta t_{n+1}}[\cos(\overline{\varphi})]\\
&-\frac{u_{\varphi,b}^C(t_{n+1})-u_{\varphi,b}^C(t_n)}{\Delta t_{n+1}}[\sin(\overline{\varphi})]-\frac{R\theta_{z,b}^C(t_{n+1})-R\theta_{z,b}^C(t_n)}{\Delta t_{n+1}}[\sin(\overline{\varphi})]\\
&=+\mathcal{I}_{N\to r}(\overline{\varphi})\left\{\sum_{i=0}^{n}\frac{N_p(t_{i+1})-N_p(t_i)}{\Delta t_{i+1}}\left[\frac{\eta}{E_c(\xi(t_n))}\frac{\beta}{t_0^*}\left(\frac{t_{n+1}-t_i}{t_0^*}\right)^{\beta-1}\right.\right.\\
&\left.\left.+\frac{\eta}{E_c(\xi(t_{n+1}))}\frac{\beta}{t_0^*}\left(\frac{t_{n+1}-t_i}{t_0^*}\right)^{\beta-1}\right]\frac{\Delta t_{i+1}}{2}+\frac{N_p(t_{n+1})-N_p(t_n)}{E(\xi(t_{n+1}))\Delta t_{n+1}}\right\}\\
&+\sum_{j=1}^{4}\left\{\mathcal{I}_{i\to r}(\overline{\varphi})\left\{\sum_{i=0}^{n}\frac{G_{p,j}(t_{i+1})-G_{p,j}(t_i)}{\Delta t_{i+1}}\left[\frac{\eta}{E_c(\xi(t_n))}\frac{\beta}{t_0^*}\left(\frac{t_{n+1}-t_i}{t_0^*}\right)^{\beta-1}\right.\right.\right.\\
&\left.\left.\left.+\frac{\eta}{E_c(\xi(t_{n+1}))}\frac{\beta}{t_0^*}\left(\frac{t_{n+1}-t_i}{t_0^*}\right)^{\beta-1}\right]\frac{\Delta t_{i+1}}{2}+\frac{G_{p,j}(t_{n+1})-G_{p,j}(t_n)}{E(\xi(t_{n+1}))\Delta t_{n+1}}\right\}\right\},
\end{aligned}
\tag{12}
$$

$$
\begin{aligned}
&+\frac{u_\varphi^C(\xi,\overline{\varphi},t_{n+1})-u_\varphi^C(\xi,\overline{\varphi},t_n)}{\Delta t_{n+1}}+\frac{u_{r,b}^C(t_{n+1})-u_{r,b}^C(t_n)}{\Delta t_{n+1}}[\sin(\overline{\varphi})]\\
&-\frac{u_{\varphi,b}^C(t_{n+1})-u_{\varphi,b}^C(t_n)}{\Delta t_{n+1}}[\cos(\overline{\varphi})]-\frac{R\theta_{z,b}^C(t_{n+1})-R\theta_{z,b}^C(t_n)}{\Delta t_{n+1}}[\cos(\overline{\varphi})-1]\\
&=+\mathcal{I}_{N\to\varphi}(\overline{\varphi})\left\{\sum_{i=0}^{n}\frac{N_p(t_{i+1})-N_p(t_i)}{\Delta t_{i+1}}\left[\frac{\eta}{E_c(\xi(t_n))}\frac{\beta}{t_0^*}\left(\frac{t_{n+1}-t_i}{t_0^*}\right)^{\beta-1}\right.\right.\\
&\left.\left.+\frac{\eta}{E_c(\xi(t_{n+1}))}\frac{\beta}{t_0^*}\left(\frac{t_{n+1}-t_i}{t_0^*}\right)^{\beta-1}\right]\frac{\Delta t_{i+1}}{2}+\frac{N_p(t_{n+1})-N_p(t_n)}{E(\xi(t_{n+1}))\Delta t_{n+1}}\right\}\\
&+\sum_{j=1}^{4}\left\{\mathcal{I}_{i\to\varphi}(\overline{\varphi})\left\{\sum_{i=0}^{n}\frac{G_{p,j}(t_{i+1})-G_{p,j}(t_i)}{\Delta t_{i+1}}\left[\frac{\eta}{E_c(\xi(t_n))}\frac{\beta}{t_0^*}\left(\frac{t_{n+1}-t_i}{t_0^*}\right)^{\beta-1}\right.\right.\right.\\
&\left.\left.\left.+\frac{\eta}{E_c(\xi(t_{n+1}))}\frac{\beta}{t_0^*}\left(\frac{t_{n+1}-t_i}{t_0^*}\right)^{\beta-1}\right]\frac{\Delta t_{i+1}}{2}+\frac{G_{p,j}(t_{n+1})-G_{p,j}(t_n)}{E(\xi(t_{n+1}))\Delta t_{n+1}}\right\}\right\},
\end{aligned}
\tag{13}
$$

$$
\begin{aligned}
&+\frac{\theta_z^C(\xi,\overline{\varphi},t_{n+1})-\theta_z^C(\xi,\overline{\varphi},t_n)}{\Delta t_{n+1}}-\frac{\theta_{z,b}^C(t_{n+1})-\theta_{z,b}^C(t_n)}{\Delta t_{n+1}}\\
&=+\mathcal{I}_{N\to z}(\overline{\varphi})\left\{\sum_{i=0}^{n}\frac{N_p(t_{i+1})-N_p(t_i)}{\Delta t_{i+1}}\left[\frac{\eta}{E_c(\xi(t_n))}\frac{\beta}{t_0^*}\left(\frac{t_{n+1}-t_i}{t_0^*}\right)^{\beta-1}\right.\right.\\
&\left.\left.+\frac{\eta}{E_c(\xi(t_{n+1}))}\frac{\beta}{t_0^*}\left(\frac{t_{n+1}-t_i}{t_0^*}\right)^{\beta-1}\right]\frac{\Delta t_{i+1}}{2}+\frac{N_p(t_{n+1})-N_p(t_n)}{E(\xi(t_{n+1}))\Delta t_{n+1}}\right\}\\
&+\sum_{j=1}^{4}\left\{\mathcal{I}_{i\to z}(\overline{\varphi})\left\{\sum_{i=0}^{n}\frac{G_{p,j}(t_{i+1})-G_{p,j}(t_i)}{\Delta t_{i+1}}\left[\frac{\eta}{E_c(\xi(t_n))}\frac{\beta}{t_0^*}\left(\frac{t_{n+1}-t_i}{t_0^*}\right)^{\beta-1}\right.\right.\right.\\
&\left.\left.\left.+\frac{\eta}{E_c(\xi(t_{n+1}))}\frac{\beta}{t_0^*}\left(\frac{t_{n+1}-t_i}{t_0^*}\right)^{\beta-1}\right]\frac{\Delta t_{i+1}}{2}+\frac{G_{p,j}(t_{n+1})-G_{p,j}(t_n)}{E(\xi(t_{n+1}))\Delta t_{n+1}}\right\}\right\}.
\end{aligned}
\tag{14}
$$

4 APPLICATION TO A BENCHMARK EXAMPLE: SIEBERG TUNNEL

The analytical mechanics model for an aging viscoelastic cylindrical shell segment, as written in Section 2 and 3 is applied to a benchmark example in NATM tunneling, which has been analyzed by various types of "hybrid methods" (Hellmich et al. 2001 and Ullah et al. 2012).

4.1 Geometrical and material properties

For the analysis of the Sieberg tunnel, constructed in the 1990s as part of the high-speed railway line connecting Vienna and Salzburg, the cross section MC1452 with radius R = 6.20 m, thickness h = 0.30 m, and opening angle $\Delta\varphi$ = 2.92 rad = 167.30°, was chosen. During the top heading excavation and installation stage, the young tunnel shell was equipped with three optical reflectors delivering displacement vectors of three measurement points (MPs), MP1, MP2, and MP3; and we here consider the corresponding measurements over the first 21 days of the lifetime of the Sieberg tunnel, see (Scharf et al. 2022). Moreover, we consider a typical shotcrete mixture with the cement type CEM II/A-S 42.5R, and the strength class SpC 20/25.

4.2 Determination of the unknowns: ground pressure, axial force, and generator rotations at the ends of the circular segment

The preceding developments contain seven unknowns, four values for the ground pressure at different locations, one value for the axial force, and two values for the generator rotations at the beginning and at the end of the circular tunnel shell segment, respectively. For the determination of these unknowns, seven equations are necessary. They are obtained as follows

- Two equations result from specification of the natural boundary condition (2) for the beginning of the arch segment and for the end of the arch segment.
- Two equations result from specification of the discretized format of the radial displacements according to Eq. (12) for the positions of MP2 and MP3.
- Two equations result from specification of the discretized format of the tangential displacements according to Eq. (13) again for the positions of MP2 and MP3.
- One equation result from specification of the discretized format of the rotation angle according to Eq. (14) for the end of the arch segment.

For the geometrical and material properties and the displacement measurements, the unknowns can be determined with the above linear system of equations, and this allows for the description of the force and stress quantities, together with the utilization degree, as well as the description of the displacement and strain quantities between the measurement points, and of the external loads, i.e., ground pressure and imposts, see (Scharf et al. 2022) and Figure 1.

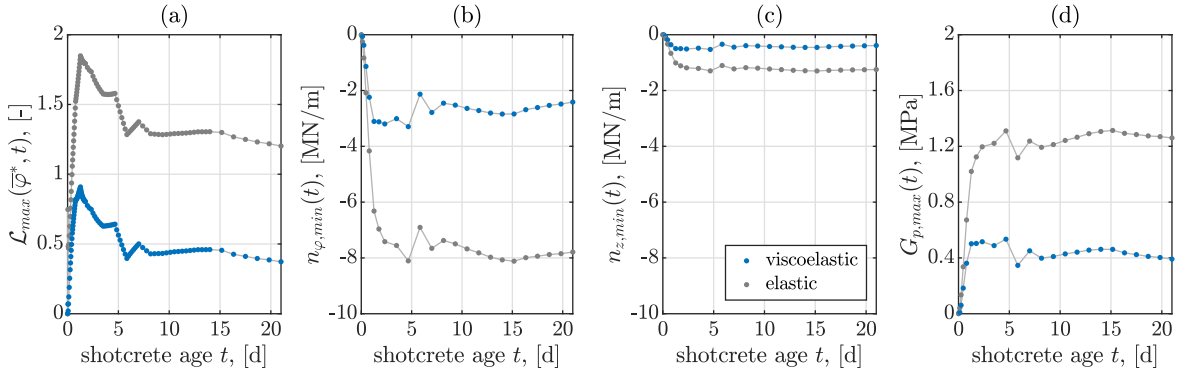

Figure 1. Comparison of elastic and viscoelastic results: history of degree of utilization (a), circumferential and axial normal force (b-c), and of ground pressure (d) of the top heading of the Sieberg tunnel, MC1452.

4.3 Role of aging creep: viscoelasticity vs. elasticity

At this point, the influence of aging creep on the degree of utilization shall be shown. More precisely, what is the effect of those terms in Eqs. (12)-(14) with sums from i = 1 to n, compared to a purely elastic evaluation, where these terms are omitted.

For the viscoelastic evaluation of a time increment $\Delta t_{n+1} = t_{n+1} - t_n$, the entire previous load history must be known and taken into account. The tunnel shell behaves more compliant compared to a purely elastic analysis. Thus, time-dependent deformation of shotcrete leads to smaller internal and external forces, see Figure 1(b)-(d), as well as to a degree of utilization which is smaller by a factor of about three, see Figure 1(a).

5 CONCLUSIONS

Consideration of polar components of point-wise measured displacement vectors in combination with a tunnel-specific shell theory and viscoelastic modeling of aging shotcrete provides analytical access to the ground pressure distribution along the tunnel circumference, impost forces, and all quantities arising from the action of the latter external forces. Purely elastic modeling would lead to unrealistically high force estimates and stresses prevailing in the tunnel structure.

ACKNOWLEDGEMENTS

The authors gratefully acknowledge project FFG-COMET #882504 “Rail4Future: Resilient Digital Railway Systems to enhance performance”.

REFERENCES

Ausweger, M., Binder, E., Lahayne, O., Reihsner, R., Maier, G., Peyerl, M. & Pichler, B. 2019. Early-Age Evolution of Strength, Stiffness, and Non-Aging Creep of Concretes: Experimental Characterization and Correlation Analysis. *Materials* 12(2), pp. 481-489.

Germain, P. 1972. Méchanique des milieux continus. *Comptes rendus de l'Académie des Sciences Série A* (t.274), pp. 1051-1055.

Germain, P. 1973. The Method of Virtual Power in Continuum Mechanics. Part 2: Microstructure. *SIAM Journal on Applied Mathematics* 25(3), pp. 556-575.

Hellmich, C., Mang, H. & Ulm, F. 2001. Hybrid method for quantification of stress states in shotcrete tunnel shells: combination of 3D in situ displacement measurements and thermochemoplastic material law. *Computers & Structures* 79(22-25), pp. 2103-2115.

Irfan-ul Hassan, M., Pichler, B., Reihsner, R. & Hellmich, C. 2016. Elastic and creep properties of young cement paste, as determined from hourly repeated minute-long quasi-static tests. *Cement and Concrete Research* 82, pp. 36-49.

Königsberger, M., Irfan-ul Hassan, M., Pichler, B. & Hellmich, C. 2016. Downscaling Based Identification of Nonaging Power-Law Creep of Cement Hydrates. *Journal of Engineering Mechanics* 142(12), 16106.

Moritz, A. B., Fleckl, J., Lienhart, W., Golser, J. & Pilgerstorfer, T. 2023: Long-term monitoring of Austrian railway tunnels - A next step forward. In *15th ISRM Congress 2023 & 72nd Geomechanics Colloquium,* Schubert & Kluckner (eds), Salzburg, Austria, October 9 - 14, 2023.

Ruiz, M., Muttoni, A. & Gambarova, P. 2007. Relationship between Nonlinear Creep and Cracking of Concrete under Uniaxial Compression. *Journal of Applied Concrete Technology* 5(3), pp. 383-393.

Scharf, R., Pichler, B., Heissenberger, R., Moritz, B. & Hellmich, C. 2022. Data-driven analytical mechanics of aging viscoelastic shotcrete tunnel shells. *Acta Mechanica* 233, pp. 2989-3019.

Scheiner, S. & Hellmich, C. 2009. Continuum Microviscoelasticity Model for Aging Basic Creep of Early-Age Concrete. *Journal of Engineering Mechanics* (ASCE) 135(4), pp. 307-323.

Ullah, S., Pichler, B., Scheiner, S. & Hellmich, C. 2012. Influence of shotcrete composition on load-level estimation in NATM-tunnel shells: Micromechanics-based sensitivity analyses. *International Journal for Numerical and Analytical Methods in Geomechanics* 36, pp. 1151-1180.